ACS Chemical Neuroscience

Article

Synthesis and Preliminary Evaluations of a Triazole-cored Antagonist ([18F]N2B-0518) as PET Imaging Probe for GluN2B Subunit in the Brain

Hualong Fu, Weiting Tang, Zhen Chen, Vasily V. Belov, Genwei Zhang, Tuo Shao, Xiaofei Zhang, Qingzhen Yu, Jian Rong, Xiaoyun Deng, Wei Han, Scott Myers, Pilar Giffenig, Lu Wang, Lee Josephson, Yihan Shao, April Davenport, James Daunais, Mikhail I Papisov, Hongjie Yuan, Zijing Li, Stephen F. Traynelis, and Steven H Liang

ACS Chem. Neurosci., **Just Accepted Manuscript** • DOI: 10.1021/acschemneuro.8b00591 • Publication Date (Web): 30 Jan 2019

ACS Publications

is published by the American Chemical Society. 1155 Sixteenth Street N.W., Washington, DC 20036

Synthesis and Preliminary Evaluations of a Triazole-cored Antagonist ([^{18}F]N2B-0518) as PET Imaging Probe for GluN2B Subunit in the Brain

Hualong Fu,[†] Weiting Tang,[§,○] Zhen Chen,[†] Vasily V. Belov,[‖] Genwei Zhang,[⊥] Tuo Shao,[†] Xiaofei Zhang,[†] Qingzhen Yu,[†] Jian Rong,[†] Xiaoyun Deng,[†] Wei Han,[§,□] Scott J. Myers,[§] Pilar Giffenig,[‖] Lu Wang, [†,Δ] Lee Josephson,[†] Yihan Shao,[⊥] April T. Davenport,[#] James B. Daunais,[#] Mikhail Papisov,[‖] Hongjie Yuan,[§] Zijing Li,*[,‡] Stephen F. Traynelis,*[,§] and Steven H. Liang*[,†]

[†]Department of Radiology, Division of Nuclear Medicine and Molecular Imaging, Massachusetts General Hospital and Harvard Medical School, 55 Fruit Street, Boston, Massachusetts 02114, United States

[§]Department of Pharmacology, Emory University School of Medicine, Atlanta, Georgia 30322, United States

[○]Department of Neurology, Xiangya Hospital, Central South University, Changsha, Hunan, 410008, P. R. China

[‖]Department of Radiology, Massachusetts General Hospital, Harvard Medical School, and the Shriners Burns Hospital, Boston, Massachusetts 02114, United States

[⊥]Department of Chemistry and Biochemistry, University of Oklahoma, Norman, Oklahoma 73019, United States

[□]Department of Neurology, Children's Hospital of Chongqing Medical University, Chongqing, 400014, P. R. China

[#]Department of Physiology and Pharmacology, Wake Forest School of Medicine, Winston Salem, North Carolina 27157, United States

[Δ]Department of Nuclear Medicine and PET/CT-MRI Center, the First Affiliated Hospital of Jinan University & Institute of Molecular and Functional Imaging, Jinan University, Guangzhou 510630, P. R. China

[‡]State Key Laboratory of Molecular Vaccinology, Molecular Diagnosis & Center for Molecular Imaging and Translational Medicine, School of Public Health, Xiamen University, Xiamen 361102, P. R. China

ABSTRACT

GluN2B is the most studied subunit of *N*-methyl-D-aspartate receptors (NMDARs) and implicated in the pathologies of various central nervous system disorders and neurodegenerative diseases. As

pan NMDAR antagonists often produce debilitating side effects, new approaches in drug discovery have shifted to subtype-selective NMDAR modulators, especially GluN2B-selective antagonists. While positron emission tomography (PET) studies of GluN2B-selective NMDARs in the living brain would enable target engagement in drug development and improve our understanding in the NMDAR signaling pathways between normal and disease conditions, a suitable PET ligand is yet to be identified. Herein we developed an ^{18}F-labeled potent antagonist, 2-((1-(4-[^{18}F]fluoro-3-methylphenyl)-1*H*-1,2,3-triazol-4-yl)methoxy)-5-methoxypyrimidine ([^{18}F]**13**; also called [^{18}F]N2B-0518) as a PET tracer for imaging the GluN2B subunit. The radiofluorination of [^{18}F]**13** was efficiently achieved by our spirocyclic iodonium ylide (SCIDY) method. In in vitro autoradiography studies, [^{18}F]**13** displayed highly region-specific binding in brain sections of rat and non-human primate, which was in accordance with the expression of GluN2B subunit. Ex vivo biodistribution in mice revealed that [^{18}F]**13** could penetrate the blood-brain barrier with moderate brain uptake (3.60% ID/g at 2 min) and rapid washout. Altogether, this work provides a GluN2B-selective PET tracer bearing new chemical scaffold and shows high specificity to GluN2B subunit in vitro, which may pave the way for the development of a new generation of GluN2B PET ligands.

Keywords: subtype-selective, PET imaging, GluN2B subunit, ^{18}F-labeling, spirocyclic iodonium ylide, autoradiography

INTRODUCTION

N-Methyl-D-aspartate receptors (NMDARs) are ligand-gated ion channel ionotropic glutamate receptors (iGluRs) that are fundamental to excitatory neurotransmission in the mammalian central nervous system (CNS).[1, 2] NMDARs are involved in numerous neurological disorders and neurodegenerative diseases such as ischemic insults, epilepsy, Parkinson's disease and Alzheimer's disease (AD).[3, 4] Several pan NMDAR antagonists including phencyclidine (PCP), ketamine, MK-801, Memantine, and amantadine were developed and used in the clinical setting;[5-8] however, these drugs often showed debilitating adverse effects and thus had a very narrow therapeutic window.[7, 9] Of note, NMDARs are typically assembled as tetramers containing two GluN1 subunits and two

GluN2 subunits.[10] The GluN2 subunits, which include four subtypes of GluN2A−GluN2D, have distinct developmental expression patterns in CNS and control a variety of functional properties of NMDARs.[11-13] For example, the GluN2B subunit is widespread throughout the brain with strong expression levels around birth; but in adults, becomes progressively restricted to the forebrain while barely detectable in cerebellum.[11, 12, 14, 15] This subunit endows the NMDARs with various binding sites for both positive allosteric modulators (PAM, e.g., polyamines) and subunit-selective negative allosteric modulators (NAM, e.g., ifenprodil)[8, 16-19] and thus attracts sufficient attention in drug development as a therapeutic target of high interest for various CNS pathologies, such as cerebral ischemia, acute and chronic pain, schizophrenia, and AD.[5, 7, 20, 21] The discovery of the first GluN2B-selective NMDAR antagonist, ifenprodil, provided an alternative solution for the treatment of NMDAR-related diseases.[22] Compared with the pan NMDAR antagonists, ifenprodil uses a unique activity-dependent mechanism that avoids excessive blockade by leaving transiently activated receptors relatively unaffected, which could mitigate its adverse effect at high drug doses.[18, 23-25] The finding of ifenprodil has stimulated the continuous development of other potent GluN2B-selective antagonists and several drug candidates have entered human trials, including CP-101606 (traxoprodil),[26, 27] RGH-896 (radiprodil),[8] MK-0657 (rislenemdaz),[28, 29] and EVT-101.[30] However, despite multiple clinical trials, no GluN2B-selective antagonists have been approved for use in man by FDA.[4, 8] Thus, a targeted probe that enables the understanding of in vivo molecular progress of GluN2B subunit is critical in assessing the future prospects for drug development, like facilitating drug candidates by evaluating the receptor occupancy.

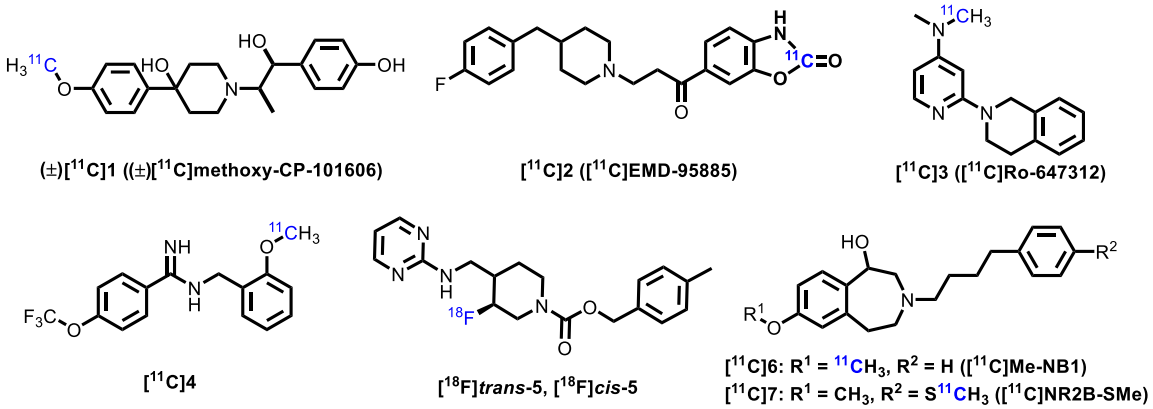

Figure 1. Chemical structures of representative GluN2B-selective NMDAR PET tracers.

Positron emission tomography (PET) imaging of NMDAR GluN2B subunit could help to diagnose and monitor related neurological disorders and further validate treatment intervention and efficacy. In parallel with drug discovery, there is an unmet clinical need for GluN2B-selective NMDAR PET tracers in basic and clinical research. There are continuous research efforts on the development of ^{11}C- or ^{18}F-labeled probes targeting the GluN2B subunit of NMDAR, which have been applied for PET imaging studies in rats or non-human primates (NHP).[31-33] Among them, ifenprodil-like ligands (±)[^{11}C]methoxy-CP-101606 ((±)[^{11}C]**1**)[34] and [^{11}C]EMD-95885 ([^{11}C]**2**, Figure 1)[35] displayed low brain uptake and homogenous distribution in different brain regions, which was inconsistent with GluN2B expression in the brain.[11, 12, 14, 15] In 2004, a pyridine derivative [^{11}C]Ro-647312 ([^{11}C]**3**, Figure 1) also showed homogenous brain distribution in rat brain and exhibited high plasma/brain uptake ratio by PET.[36] In 2006, a benzamidine derivative [^{11}C]**4** (Figure 1) demonstrated poor brain uptake and rapid metabolism in the rat brain, which impeded its further application in PET imaging.[37] Although in vitro studies revealed two ^{18}F-labeled probes [^{18}F]*trans*-**5** and [^{18}F]*cis*-**5** (Figure 1) had promising B_{max}/K_d ratios (8–37) in different rat brain regions, PET studies failed to observe significant difference of radioactivity signals in different brain regions.[38, 39] More recently, [^{11}C]Me-NB1 ([^{11}C]**6**, Figure 1) was generated from a benzo[*d*]azepin GluN2B subunit antagonist.[40] [^{11}C]**6** had high affinity (K_i = 5.3 nM) to GluN2B subunit and was successfully used in measurement of receptor occupancy by eliprodil (an NMDAR antagonist). It is worthy of note that the specific uptake of [^{11}C]**6** in rat brain was also affected by (+)-pentazocine (a σ-1

receptor agonist) and haloperidol (an inverse agonist of the σ-1 receptor) blocking studies, which was explained by the indirect effect of the σ-1 receptor in vivo. Furthermore, Cai *et al.* reported an interesting sulfur analog of benzo[*d*]azepin PET tracer [^{11}C]NR2B-SMe ([^{11}C]**7**, Figure 1).[41] In PET imaging of rats, the brain uptake of [^{11}C]**7** was reduced by the pretreatment with eliprodil, ifenprodil, and NR2B-SMe (self-blocking), as well as a σ-1 receptor agonist SA 4503 in a dose-dependent manner. Despite continuous research efforts in the development of PET ligands for this target, to date, no PET tracer of GluN2B subunit has been advanced to human study and PET imaging of GluN2B subunit remains challenging.[31-33]

Herein we developed a new series of fluorinated compounds that are amenable for ^{18}F-labeling based on a novel class of GluN2B antagonists recently disclosed from Janssen Pharmaceutical patents,[42] with the aim to discover new generation of GluN2B PET ligands with diverse chemotypes and pharmacology. Starting from an efficient parallel synthesis of several methoxypyrimidine compounds (**11**–**14**), we performed preliminary pharmacological evaluation and identified two promising molecules (**11** and **13**) with high potency and selectivity to GluN2B subunit. Molecular docking studies also indicated several key interactions including π-π stacking and hydrogen bonds were found to support our pharmacology findings. As for radiochemistry, our spirocyclic iodonium ylide (SCIDY) method[43, 44] enables rapid, efficient and modular synthesis of [^{18}F]**11** and [^{18}F]**13** in high radiochemistry yields (RCYs), which is otherwise difficult to access by traditional aromatic nucleophilic substitution. The following *in vitro* autoradiography (ARG) in brain sections of both rat and NHP demonstrated that [^{18}F]**13** could bind to GluN2B subunit with high specificity. Furthermore, ex vivo biodistribution in mice revealed that [^{18}F]**13** possessed moderate brain uptake, although short retention and fast clearance was also observed. As proof-of-concept, our work provides a preliminary evaluation of new potent and selective triazole-based PET probes targeting GluN2B subunit and may lead to new chemotypes to discover new chemical scaffolds for NMDAR drug discovery and PET tracer development.

RESULTS AND DISCUSSION

Chemistry. The synthesis of new GluN2B-selective NMDAR antagonists amenable for radiolabeling (**11**−**14**) is illustrated in Scheme 1. The synthesis of **11** commenced with the preparation of aromatic azide **9**. In acidic conditions, aniline **8** reacted with sodium nitrite and subsequently sodium azide, which resulted in diazonium salts in situ and then converted into azide **9** in a high yield of 89% over two steps. The key triazole intermediate **10** was prepared by copper(I)-induced alkyne−azide cycloaddition 'click' reactions between azidobenzene **9** and propargyl alcohol in a high yield of 71% as a white solid. Then the nucleophilic aromatic substitution (S_NAr) reaction between triazole **10** and 2-bromo-5-methoxypyrimidine afforded the target compound **11** in a moderate yield of 29%. In brief, the synthesis of **11** was efficiently achieved in three steps with an overall yield of 18%. In an analogous manner, the other target compounds **12**−**14** were obtained as white solids in overall yields of 13%−18%.

Scheme 1. Synthesis of GluN2B-selective NMDAR antagonists (**11**–**14**).

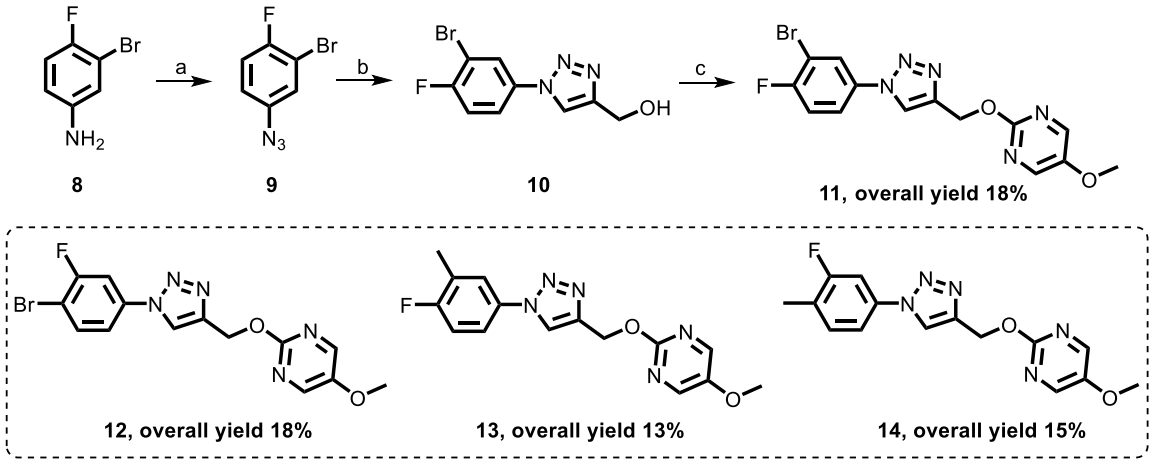

Reagents and conditions: (a) $NaNO_2$, NaN_3, HCl (6 N), 0–5 °C, 2 h, 89% yield. (b) Propargyl alcohol, DIPEA, CuI, THF, 40 °C, 2 h, 71% yield. (c) 2-Bromo-5-methoxypyrimidine, NaH, THF, 40 °C, 2–3 h, 29% yield.

Pharmacology and Physicochemical Properties.

In most cases, NMDARs are dimer of dimers containing two glycine-binding GluN1 and two glutamate-binding GluN2 subunits, and their functionating relies on joint action of glycine and glutamate.[2, 10] The potencies of compounds **11**−**14** as GluN2B-selective antagonists were evaluated

via glutamate/glycine (100 μM/100 μM) assays with *Xenopus* oocytes expressing human GluN1/GluN2B (GenBank NP_015566/GenBank NP_000825) receptors. The current responses of GluN1/GluN2B receptors were inhibited by **11**−**14** in a dose-dependent manner (Figure 2A). As shown in Table 1, **11** had the highest potency with the IC_{50} value of 19 nM, followed by **13** with the value of 28 nM. However, the potencies of **12** and **14** (positional isomers of **11** and **13**, respectively) significantly decreased to 339 and 89 nM (IC_{50} values), respectively. We also evaluated the subtype-selectivity of compounds **11** and **13** for GluN2B subunit over other GluN2 subunits. *Xenopus* oocytes expressing GluN1 with human GluN2A, rat GluN2C, or human GluN2D subunit were used, and current responses to maximal agonists (glutamate/glycine, 100 μM/100 μM) concentrations were recorded in the presence of **11** or **13** (1 μM). The activity of GluN1/GluN2B receptors was substantially inhibited by **11** and **13** with the %current responses of 9.3% and 15.0%, respectively (Table 1 and Figure 2B). In contrast, the current responses of other iGluRs including GluN1/GluN2A, GluN1/GluN2C, GluN1/GluN2D, GluA1, and GluK2 were virtually not affected by **11** or **13** (Table 1 and Figure 2B).

Two different GluN2 subunits, GluN2A and GluN2B, have been found in most NMDAR-expressing cells and are assembled as triheteromers like GluN1/GluN2A/GluN2B (2A/2B) and diheteromers like GluN1/GluN2A/GluN2A (2A/2A) and GluN1/GluN2B/GluN2B (2B/2B).[2, 45] Thus, we further compared compounds **11** and **13** inhibition of triheteromeric receptors (2A/2B) to that of diheterometric 2A/2A and 2B/2B receptors. Compounds **11** and **13** inhibited current responses from wild-type 2B/2B with an IC_{50} of 11 ± 2.3 and 20 ± 3.4 nM, maximal inhibition of 86% ± 1.8% (n = 11) and 88% ± 1.8% (n = 11), respectively, whereas responses from wild-type 2A/2A were insensitive to 1 μM **11** (n = 10) and **13** (n = 11) (Figures 2C and 2D). The inhibition of 2A/2B triheteromeric receptors by **11** and **13** (1 μM) was reduced compared to that of 2B/2B, since IC_{50} values increased to 141 ± 8.9 nM for **11** and 154 ± 28 nM for **13**, and maximal inhibition was 23% ± 2.5% (n = 11) for 11 and 27% ± 2.0% for **13** (n = 13). Similar to the effects of ifenprodil,[45] our data suggest that reduced sensitivity of triheteromers to these two compounds (**11** and **13**) is mainly mediated by a diminished maximal inhibition, in addition to reduction in potency. As a

result, **11** and **13** are identified as potent GluN2B-selective antagonists with high selectivity over other GluN2 subunits and iGluR units, representing a promising chemical scaffold for GluN2B-selective NMDAR PET ligands.

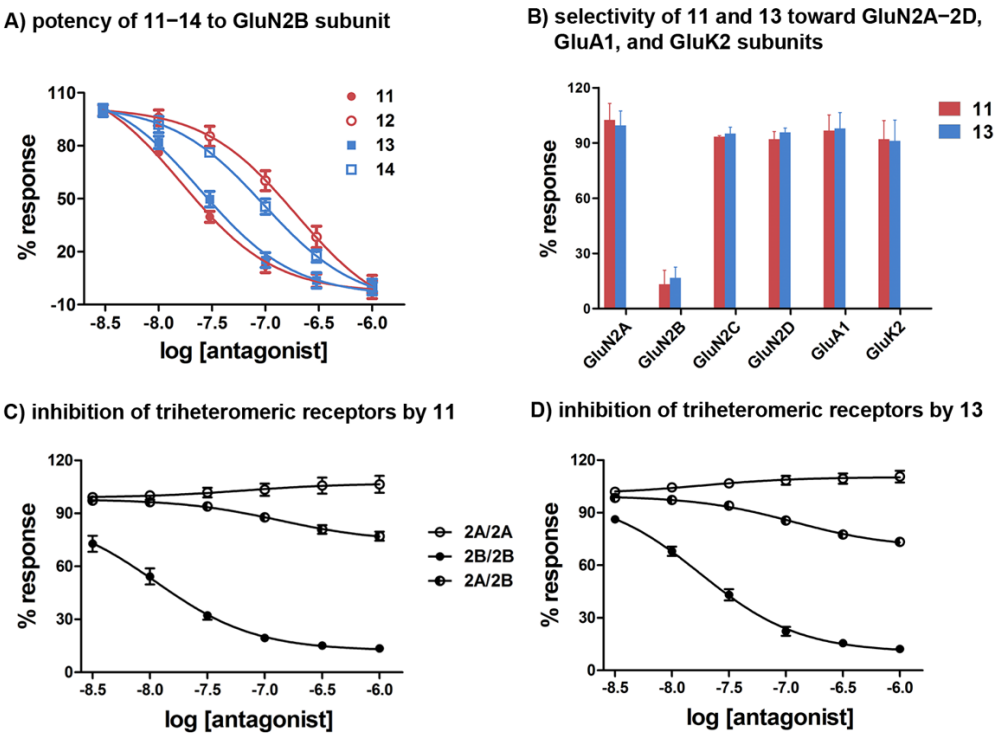

Figure 2. Pharmacology studies of our GluN2B-selective NMDAR antagonists. (A) Concentration−response curves for antagonists **11**−**14** (0.03−1.0 μM) on human GluN1/GluN2B were plotted as the percent of the maximal response to glutamate/glycine (100 μM/100 μM) and fit by the Hill equation. (B) %Current responses to glutamate/glycine (100 μM/100 μM for NMDAR) or glutamate (100 μM for AMPAR and KAR) co-applied with compound solution (1 μM) of **11** or **13** were recorded in *Xenopus* oocytes expressing human GluN1/GluN2A receptors, human GluN1/GluN2B receptors, human GluN1/GluN2D receptors, rat GluN1/GluN2C receptors, rat GluA1(flip) subunit or rat GluK2(Q) subunit. The data were expressed as the percent of the maximal response to agonists. (C and D) Inhibition of triheteromeric receptors by compounds **11** (C) and **13** (D), respectively. Concentration−response curves were generated from the triheteromeric receptors including GluN1/GluN2A/GluN2A (2A/2A), GluN1/GluN2B/GluN2B (2B/2B), and GluN1/GluN2A/GluN2B (2A/2B) upon activated by glutamate/glycine (100 μM/100 μM). Data are mean ± SEM from

10–14 oocytes.

Table 1. Potency and selectivity of compounds **11**−**14**

entry	potency[a]	selectivity[b]					
	IC_{50}, mean (nM) pIC_{50}, mean (95% CI)	%control at 1 μM, mean (99% CI)					
		GluN2A	GluN2B	GluN2C	GluN2D	GluA1	GluK2
11	19 -1.72 (-1.75, -1.69)	102 (93, 111)	13 (7, 19)	93 (92, 94)	92 (88, 96)	97 (90, 104)	92 (84, 100)
12	339 -0.55 (-0.76, -0.34)	n.d.					
13	28 -1.57 (-1.63, -1.51)	99 (93, 105)	17 (11, 23)	95 (92, 98)	96 (94, 98)	98 (91, 105)	91 (80, 102)
14	89 -1.12 (-1.30, -0.94)	n.d.					

[a]Determined with *Xenopus* oocytes expressing human GluN1/GluN2B receptors in 100 μM glutamate/glycine assay coapplied with increasing concentrations of **11**−**14** (n = 6−12). [b]%Control response was expressed as the percent of the maximal response to 100 μM glutamate/glycine (for GluN2a-GluN2D subunits), or to 100 μM glutamate (for GluA1 and GluK2 subunits). *Xenopus* oocytes coexpressing human GluN1/GluN2A receptors, human GluN1/GluN2B receptors, human GluN1/GluN2D receptors, rat GluN1/GluN2C receptors, rat GluA1(flip) subunit or rat GluK2(Q) subunit were used. n.d., not determined.The lipophilicity with preferred range of 2.0−3.5 in candidate compounds is an empirical factor that could predict the ability of the blood-brain barrier (BBB) penetration.[46-48] The calculated logP (clogP) values of **11**−**14** are 3.32, 3.32, 2.90, and 2.90, respectively (Table 2). The logD values of [^{18}F]**11** and [^{18}F]**13** (see radiochemistry below, Scheme 2) were determined to be 3.14 and 2.89 by "shake-flask" method,[49] respectively, which are within the optimal range for BBB permeability. In silico prediction gave a reasonable topological polar surface area (tPSA) value of 71.4 Å (<90 Å) for all the compounds (Table 2), which indicated their great potentials as brain penetrant leads.[50] We also explored the CNS PET multiparameter optimization (MPO) scores of these compounds. As reported, a higher MPO score of a compound often leads to a higher probability in achieving optimal CNS drug-like properties such as

permeability, clearance, and safety.[51, 52] As shown in Table 2, **13** and **14** had preferred MPO scores >4.9 while **11** and **12** exhibited a lower value of 4.05. It is worth mentioning that compound **13** has the highest MPO score of 5.16, which is situated in the optimal range (>5) that is characteristic of successful PET ligands.[53] These results led to further evaluations of [^{18}F]**13** in in vitro ARG and ex vivo biodistribution studies.

Table 2. Physicochemical properties of compounds **11**−**14**.

compound	clogP[a]	log$D_{7.4}$[b]	tPSA (Å)[a]	MPO[c]
11	3.32	3.14 ± 0.037	71.4	4.05
12	3.32	n. d.	71.4	4.05
13	2.90	2.89 ± 0.037	71.4	5.16
14	2.90	n. d.	71.4	4.91

[a]ClogP and tPSA values were calculated by ChemBioDraw Ultra 14.0. [b]LogD was measured with "shake-flask" method by using corresponding ^{18}F-labeled tracers (18.5 MBq) and expressed as mean ± SD (n = 3). [c]MPO scores were calculated using the method reported in Zhang, L.et al. [53]. n. d., not determined.

Molecular Docking Studies

A 2.6-Å resolution crystal structure of the NMDA receptor subunit GluN1b and GluN2B complex was downloaded (PDB ID: 3QEL)[18] and the original ligand, ifenprodil, was removed before performing the molecular docking studies. The goal is to identify possible and preliminary molecular interaction between our GluN2B inhibitors 11 & 13 and binding domain based on the fact that low nanomolar binding affinities were identified. First, we reproduced the binding pose of the original ligand, ifenprodil, within 3QEL using AutoDock Vina, which yielded a nearly-perfect overlapping between the docked pose and original pose (RMSD = 0.36 Å). Subsequently, candidate compounds **11** and **13** were docked onto the 3QEL structure in the ifenprodil site. A consensus binding pose with highest docking scores was found for these two compounds within the ifenprodil binding channel, which is the interface between subunits GluN1b and GluN2B (Figure 3). Inside the binding pocket, angled π-π stacking interactions were observed between the phenyl group of either compound and nearby Phe429 and Tyr82 side chains (Figure 3). Multiple hydrogen bonds

were also found between the pyrimidine moiety of the compounds and Arg88 side chain. In addition, the charged side chain of Glu421 was found ~3Å away from both compounds, indicating possible electrostatic interactions. The high docking scores of **11** and **13** (-9.1 and -9.4, respectively) indicated strong bindings between the compounds and NMDAR subunit, which agree well the experimental IC_{50} data in Table 1. Overall, this preliminary docking study showed that compounds **11** and **13** interacted with NMDAR subunit at the ifenprodil site with π-π stacking interactions, hydrogen bonds, and possibly electrostatic interactions.

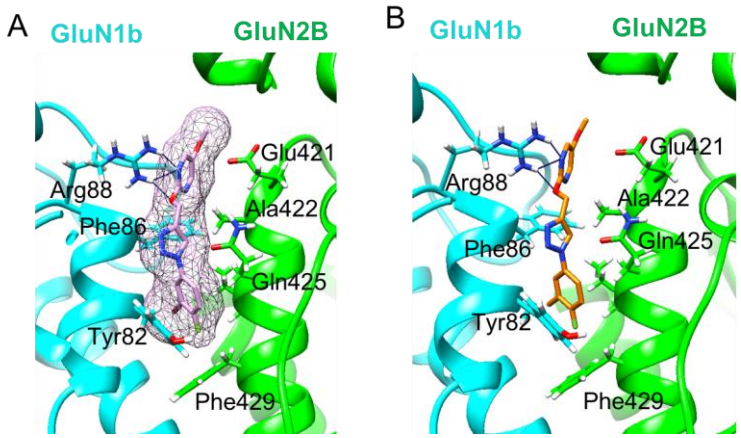

Figure 3. Molecular docking structures of compounds **11** (purple in A) and **13** (orange in B) onto NMDAR subunit GluN1b and GluN2B interface.

Radiochemistry. S_NAr reactions with $[^{18}F]F^-$ is one of the widely used and highly attractive methods for the synthesis of ^{18}F-labeled aromatic PET ligands.[54] In our initial design of the labeling strategy, we took advantage of S_NAr reactions to incorporate fluorine-18 into the desired compounds. As shown in Scheme 2A, compound **17** was prepared by the copper(I)-induced "click" reaction between aromatic azide **15** and intermediate **16** (the synthesis of **15** and **16** is shown in Scheme S1, Supporting Information) and used as the precursor for one-step ^{18}F-labeling, in which $-NO_2$ serves as the leaving group. However, ^{18}F-labeled compound **11** ($[^{18}F]$**11**) was obtained in poor radiochemistry yield (RCY) <3% (decay corrected) and difficult to purify by high-performance liquid chromatography (HPLC) because of overlapping impurities. The low RCY of

this method may be caused by the lack of an appropriate leaving group in **17**, i.e., an electron-withdrawing group at its ortho or para position.[55, 56] As our alternative strategy, we explored a step-wise synthesis of [^{18}F]**11** and [^{18}F]**13** using SCIDY method[43, 44] (Scheme 2B). The corresponding precursors **20** and **21** were prepared from the oxidation of iodinated azidobenzenes (**18** and **19**, the synthesis is shown in Scheme S1, Supporting Information) with mCPBA, followed by ligand exchange with SPIAd[44] in the same overall yields of 36%. As illustrated in Scheme 2B, the radiolabeling commenced with the generation of [^{18}F]**9** and [^{18}F]**22**, and the subsequent step was accomplished by "click" reaction between ^{18}F-labeled azidobenzenes ([^{18}F]**9** and [^{18}F]**22**) and **16**, which afforded [^{18}F]**11** and [^{18}F]**13** in high overall isolated RCYs of 35% and 39% (n = 5, decay corrected), respectively. The products of [^{18}F]**11** and [^{18}F]**13** were generated in high radiochemistry purity >99% and good molar activity of ~19 GBq/μmol (n = 5) for [^{18}F]**13** and ~6 GBq/μmol for [^{18}F]**11** (n = 5). Furthermore, since the 1,2,3-triazole linker showed good biostability in vivo and is used as an isosteric surrogate for peptide bond,[57] our radiolabeling method may provide a highly-efficient modular synthesis route for the preparation of new ^{18}F-arene click agents.

Scheme 2. Synthesis of the precursors (**17**, **20**, and **21**) and radiosynthesis of [^{18}F]**11** and [^{18}F]**13**.

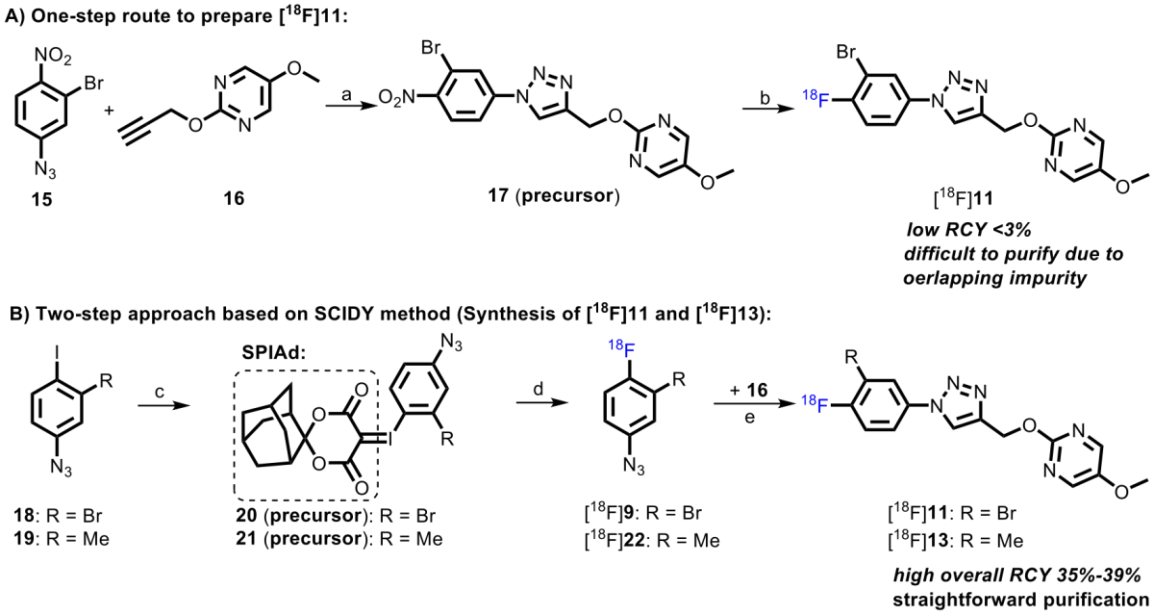

Reagents and conditions: (a) DIPEA, CuI, THF, 40 °C, 4 h, 25% yield. (b) [^{18}F]F$^-$, Kryptofix$_{222}$/K_2CO_3 (7.5/1.5 mg), anhydrous DMF, 140 °C, 10 min, <3% yield (decay corrected). (c) 1) *m*CPBA, $CHCl_3$, rt, overnight; 2) SPIAd, Na_2CO_3 (10%), ethanol, pH = 10, rt, 6 h, 36% yield over two steps. (d) [^{18}F]F$^-$, TEAB, anhydrous DMF, 120 °C, 10 min. (e) DIPEA, CuI, anhydrous DMF, 100 °C, 10 min, 35% and 39% yield for [^{18}F]**11** and [^{18}F]**13**, respectively, over two steps (decay corrected).

In Vitro Autoradiography. The GluN2B subunit is widespread throughout the CNS with high expression in the forebrain including cortex, hippocampus, and thalamus, while barely detectable in the cerebellum.[11, 12, 14, 15] To assess the specificity of the new tracer to GluN2B subunit, we used [^{18}F]**13** (with higher MPO score and lower lipophilicity compared to [^{18}F]**11**) to perform in vitro ARG on the brain cryosections (20 μm) of both rat and NHP. As shown in Figure 3A, the radioactivity of [^{18}F]**13** in rat brain sections showed brain region-specific localization (heterogeneous distribution), in which the uptake was the highest in hippocampus and cortex (especially orbital, prelimbic, and somatomotor areas), moderate in striatum and thalamus, and low in the cerebellum. This distribution pattern was in accordance with the in vitro autoradiograms of [^{3}H]CP-101606,[58] (±)[^{11}C]**1**,[34] and [^{18}F]*cis*-**5**,[38] as well as with mRNA distribution of GluN2B subunit.[59] In self-blocking experiments, the uptake of [^{18}F]**13** was substantially reduced (~90%) in the presence of cold compound **13** (10 μM, Figure 3C, also see Figure S3 in SI for self-blocking results at 1 μM) and the specific binding of [^{18}F]**13** was 94%, 94%, 92%, and 88% ($n = 3$, $p < 0.001$, T-test, Figure 3E) in brain regions of hippocampus, frontal cortex, striatum, and thalamus, respectively. The specificity of [^{18}F]**13** to GluN2B subunit was further confirmed by using a GluN2B-selective NAM, the ifenprodil derivative BMT-108908 (K_i = 1.4 nM),[60, 61] and the results showed that the binding of [^{18}F]**13** was strongly inhibited by this drug (Figure 3D and 3E) in a similar pattern of self-blocking. This result also indicated that [^{18}F]**13** associated with GluN2B subunit in the same binding site as BMT-108908, which was also confirmed by the molecular docking results (Figure 3).

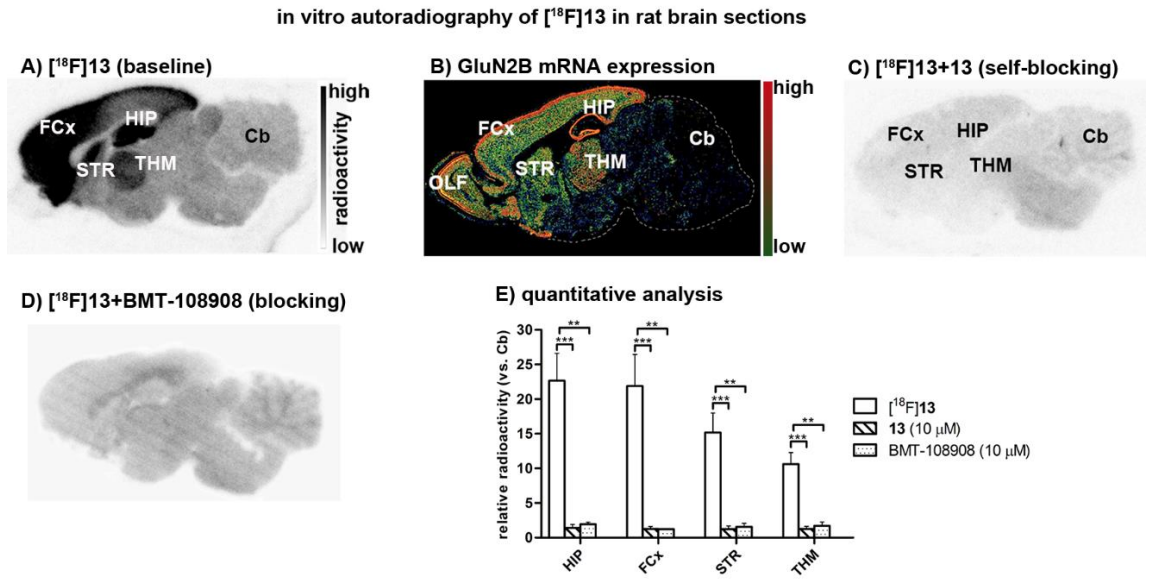

Figure 3. In vitro autoradiography results of [^{18}F]**13** (37 kBq/mL, 1.58 nM) in rat brain sections. Representative autoradiograms in rat brain sagittal sections: [^{18}F]**13** alone (A, baseline), and pre-blocked by cold compound **13** (C, self-blocking, 10 μM) and BMT-108908 (D, a NAM drug blocking, 10 μM). (B) GluN2B mRNA expression in mouse brain and the data were retrieved from mouse.brain-map.org (experiment: 69257725). (E) Quantitative analysis of baseline and blocking experiments. The value is expressed as the ratio of the radioactivity of different brain regions to that of the cerebellum (reference region). HIP, hippocampus; FCx, frontal cortex; STR, striatum; THM, thalamus; Cb, cerebellum; OLF, olfactory bulb. Asterisks indicate statistical significance: ***p <0.001, and **p <0.01 vs control.

Given the high specificity of [^{18}F]**13** to GluN2B subunit, we further explored the distribution pattern of GluN2B subunit in the NHP brain. Figure 4A showed that the highest bound activity of [^{18}F]**13** was found in brain regions of the hippocampus, entorhinal cortex, and insular cortex. The activity was moderate in caudate nucleus and putamen, low in the thalamus and claustrum, and no appreciable binding in white matter of forebrain. The nonspecific binding was determined by self-blocking studies using non-radioactive **13** (10 μM, Figure 4B) and the results showed that the radioactivity of [^{18}F]**13** distributed to several brain regions with high specificity including hippocampus (87%, n = 3, p <0.001, T-test, Figure 4D), entorhinal cortex (89%, p <0.01), insular cortex (82%, p <0.001), caudate nucleus (79%, p <0.01), and putamen (73%, p <0.01), but lower

in thalamus (53%, p <0.01). The specific binding to NMDAR GluN2B subtype was further confirmed by the blocking experiments with BMT-108908 (10 μM)[60, 61] and the %blockade results were similar to those of self-blocking studies (Figure 4C and 4D). In summary, [^{18}F]**13** showed high specific binding to GluN2B subunit in the NHP brain sections, which showed characteristic and regional-specific GluN2B subunit expression and target specificity (validated by blocking studies).

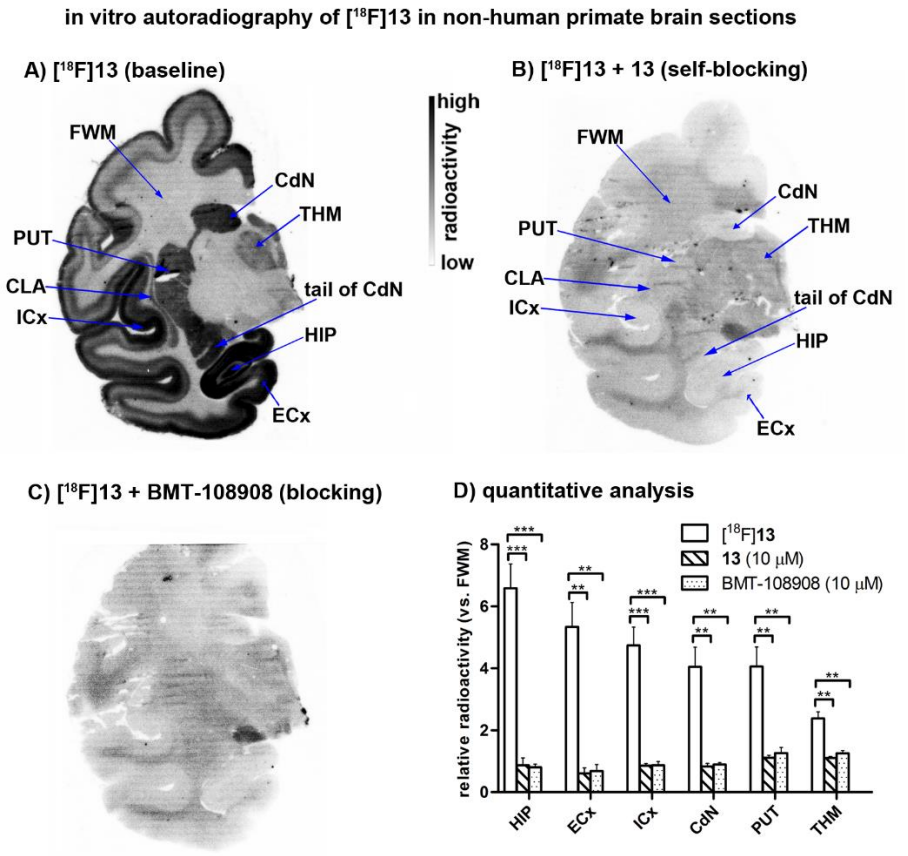

Figure 4. In vitro autoradiography results of [^{18}F]**13** (37 kBq/mL, 1.58 nM) in NHP brain sections. Representative autoradiograms in NHP brain sections: [^{18}F]**13** alone (A, baseline), and pre-blocked by cold compound **13** (B, self-blocking, 10 μM) and BMT-108908 (C, a NAM drug blocking, 10 μM). (D) Quantitative analysis of baseline and blocking experiments. The value is expressed as the ratio of the radioactivity of different brain regions to that of the white matter of forebrain. HIP, hippocampus; ECx, entorhinal cortex; ICx, insular cortex; CdN, caudate nucleus; CLA, claustrum; PUT, putamen; THM, thalamus; FWM, white matter of forebrain. Asterisks indicate statistical significance:

***p <0.001, and **p <0.01 vs control.

Whole Body Ex Vivo Biodistribution Studies and Radiometabolite Analysis. GluN2B antagonist **13** exhibited a favorable MPO score (5.16), proper lipophilicity ($logD_{7.4}$ 2.89) and reasonable polar surface area (71.4 Å), indicating a high probability to be a successful PET tracer. We next performed whole body ex vivo biodistribution studies to examine the uptake, distribution and clearance of [^{18}F]**13** in organs of interest. The studies were conducted in mice at four different time points (2, 10, 30, and 60 min) after the injection of [^{18}F]**13**. As shown in Figure 5A, several organs including heart, lung, kidney, liver, and small intestine showed high initial uptakes (> 5% ID/g) of [^{18}F]**13** at 2 min postinjection. After initial uptake, the radioactivity in organs/tissues of heart, lung, kidney, spleen, pancreas, and muscle displayed rapid washout with the uptake <0.6% ID/g at 60 min postinjection, while the levels in liver (20.84% ID/g) and small intestine (39.15% ID/g) remained high until 10 min post injection and then decreased rapidly (Figure 5A and Table S1 in Supporting Information). These results indicated that [^{18}F]**13** probably underwent hepatobiliary elimination. Of note, [^{18}F]**13** displayed reasonable initial brain uptake ($brain_{2min}$) with the value of 3.60 %ID/g, followed by a very rapid washout to 0.72 %ID/g at 10 min post injection, then to 0.018% ID/g at 60 min post injection (Figure 5B). The uptake in blood was higher than that in the brain at all time points (Figure 5). As a result, the observed abnormal rapid clearance of [^{18}F]**13** in the brain ($brain_{2min}/brain_{10min}$ = 5, and $brain_{2min}/brain_{60min}$ = 200) diminished our enthusiasm in pursuing in vivo PET evaluation in rodents. Notably, no substantial bone uptake of [^{18}F]**13** was observed (<2 %ID/g, Figure 4B), indicating little defluorination occurred in vivo. In addition, probe [^{18}F]**11** with higher lipophilicity ($logD_{7.4}$ 3.14) displayed similar biodistribution results as [^{18}F]**13** (Table S1) in different organs. In particular, [^{18}F]**11** showed lower initial brain uptake ($brain_{2min}$ = 3.27% ID/g) and slower brain washout ($brain_{2min}/brain_{60min}$ = 55).

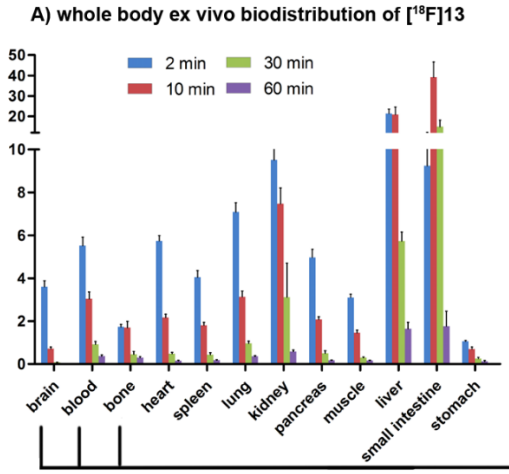

B) brain, blood, and bone uptakes of [^{18}F]13

time (min)	uptake (% ID/g)		
	bone	blood	brain
2	1.73 ± 0.12	5.52 ± 0.39	3.60 ± 0.28
10	1.69 ± 0.30	3.04 ± 0.32	0.72 ± 0.078
30	0.46 ± 0.13	0.92 ± 0.13	0.084 ± 0.0076
60	0.29 ± 0.063	0.37 ± 0.060	0.018 ± 0.0036

Figure 5. (A) Ex vivo biodistribution in mice at four different time points (2, 10, 30, and 60 min) post injection of [^{18}F]**13**. The results are expressed as the percentage of the injected dose per gram of wet tissue (% ID/g) with the exception that stomach uptake was expressed as % ID/organ. (B) The values of the brain, blood, and bone uptakes of [^{18}F]**13**. The values for remaining organs of interest are included in Table S1 of Supporting Information.

To further understand the pharmacokinetics of [^{18}F]**13**, the metabolism studies in ICR mice (n = 2) were carried out by radioHPLC analysis of plasma, brain, and liver extracts at 15 min post injection. The results showed that [^{18}F]**13** displayed moderate stability in the brain with 56.6% parent fraction left. In contrast, this probe degraded to a greater extent in plasma and liver with 11.8% and 5.1% parent fraction remained, respectively. Only polar radiometabolites of [^{18}F]**13** were found in plasma, brain, and liver. In addition, [^{18}F]**11** exhibited better stability than [^{18}F]**13** in mice with 84.8%, 32.0%, and 17.7% parent tracer remained in brain, plasma, and liver, respectively, at 15 min post injection. The results indicated that both [^{18}F]**11** and [^{18}F]**13** underwent moderate metabolism in the brain but rapid degradation in plasma and liver, which may contribute to the moderate brain uptake seen in the ex vivo biodistribution studies.

Conclusion

In this report, we successfully designed and synthesized a series of GluN2B-selective NMDAR antagonists (**11**–**14**) with the chemical scaffold containing triazole and methoxypyrimidine groups.

Two compounds, **11** and **13**, showed high potency and high selectivity to GluN2B subunit in in vitro glutamate/glycine assays with *Xenopus* oocytes, which identified them as potent candidates for PET ligand development. Molecular docking studies also identified the binding of both compounds to the interface between GluN1 and GluN2B subunits. In silico prediction showed that **11** and **13** had optimal clogP and tPSA values for CNS drug discovery and **13** exhibited the highest MPO score (5.16), indicating its great potential for PET imaging studies. Our SCIDY method enables an efficient radiosynthesis of [^{18}F]**11** and [^{18}F]**13** (also called [^{18}F]N2B-0518) in high RCYs (>35%). The following in vitro ARG in rat brain sections unveiled the specific binding of [^{18}F]**13** in brain regions of the hippocampus, frontal cortex, striatum, and thalamus, but not cerebellum, which is in accordance with the expression of GluN2B subunit. Furthermore, autoradiograms of [^{18}F]**13** in NHP brain sections demonstrated that the GluN2B subunit expressed strongly in the hippocampus, entorhinal cortex, insular cortex, caudate nucleus, and putamen, moderately in claustrum and thalamus. Ex vivo biodistribution in mice showed that [^{18}F]**13** penetrated the brain with moderate initial uptake and rapid washout, which may be attributed to poor biostability of [^{18}F]**13** in the plasma. Further PET imaging work of [^{18}F]**13** in higher species will be planned to investigate if inter-species differences exist in the brain uptake and metabolic rate in the plasma. In summary, we provided a potent and selective PET ligand for in vitro detection of GluN2B subunit, which not only widens the landscape of PET probes targeting GluN2B subunit but also offers a new structural framework for medicinal chemistry design.

METHODS

General Information. All chemicals were purchased from commercial vendors and used without further purification unless otherwise indicated. Thin-layer chromatography (TLC) was conducted with 0.25 mm silica gel plates ($^{60}F_{254}$) and visualized by exposure to UV light (254 nm) or by staining with potassium permanganate. Column chromatography purification was performed using silica gel (SiliCycle Inc., 230−400 mesh, 40−63 μm). ^{1}H, ^{13}C, and ^{19}F NMR were obtained at 300, 75, and 282 MHz, respectively, on a Bruker spectrometer in $CDCl_3$ or d_6-DMSO solutions at room

temperature, and the chemical shifts were quoted in δ values (parts per million, ppm) downfield relative to the internal TMS. The multiplicities are abbreviated as follows: s = singlet, d = doublet, t = triplet, q = quartet, m = multiplet, br = broad signal, and dd = doublet of doublets. For LC-MS, the ionization method is ESI using Agilent 6430 Triple Quad LC/MS. The compounds **11**–**14** did not show any promiscuous moieties in the Pan Assay Interference Compounds Assay (PAINS) using the *in silico* filter (http://www.swissadme.ch/index.php).[62, 63] The animal experiments were approved by the Institutional Animal Care and Use Committee of Massachusetts General Hospital. CD1 (ICR) mice (female; 8 weeks, 23-27 g) were kept on a 12 h light/12 h dark cycle and were allowed food and water adlibitum.

Chemistry.

*4-Azido-2-bromo-1-fluorobenzene (**9**)*. Compound **9** was prepared by a previously reported procedure.[64] Dark brown oil, yield 89%. ^{1}H NMR (300 MHz, $CDCl_3$) δ 7.22 (d, J = 2.6 Hz, 1H), 7.10 (t, J = 8.2 Hz, 1H), 6.95 – 6.93 (m, 1H). ^{13}C NMR (75 MHz, $CDCl_3$) δ 156.38 (d, J = 245.6 Hz), 136.85, 123.70, 119.29 (d, J = 7.1 Hz), 117.28 (d, J = 24.0 Hz), 109.97 (d, J = 22.6 Hz). ^{19}F NMR (282 MHz, $CDCl_3$) δ -108.03 – -108.05 (m).

*(1-(3-Bromo-4-fluorophenyl)-1H-1,2,3-triazol-4-yl)methanol (**10**)*. To a solution of compound **9** (2.0 g, 9.3 mmol) in THF (20 mL) was added propargyl alcohol (1.0 g, 18.0 mmol) and DIPEA (244 mg, 1.9 mmol), and then CuI (88 mg, 0.5 mmol) was added under stirring. The reaction mixture was stirred at 40 °C for 2 h. Upon completion the reaction mixture was filtered, and the solvent was removed under vacuum. The residue was purified via silica gel column chromatography using a gradient mixture of hexane–ethyl acetate (50%–100%) to obtain the pure compound of **10** as white solid (1.8 g, 6.6 mmol, 71%). ^{1}H NMR (300 MHz, d_6-DMSO) δ 8.73 (s, 1H), 8.30 (d, J = 2.7 Hz, 1H), 7.99 (d, J = 4.2 Hz, 1H), 7.61 (t, J = 8.7 Hz, 1H), 5.34 (s, 1H), 4.60 (s, 2H). ^{13}C NMR (75 MHz, d_6-DMSO) δ 158.26 (d, J = 246.1 Hz), 149.76, 134.39 (d, J = 3.1 Hz), 125.24, 121.79, 121.69, 118.26 (d, J = 24.0 Hz), 109.54 (d, J = 22.6 Hz), 55.34. ^{19}F NMR (282 MHz, d_6-DMSO) δ -104.77 – -104.80 (m).

*2-((1-(3-Bromo-4-fluorophenyl)-1H-1,2,3-triazol-4-yl)methoxy)-5-methoxypyrimidine (**11**)*.

Compound **10** (108.7 mg, 0.4 mmol) was dissolved in 10 mL THF, along with 2-bromo-5-methoxypyrimidine (50 mg, 0.3 mmol), and then NaH (70 mg, 1.7 mmol, 60% dispersion in mineral oil) was added in small portion under stirring. The reaction mixture was stirred at 40 °C for 3 h, and subsequently quenched with saturated solution of ammonium chloride. After that, the mixture was extracted with dichloromethane, and the combined organic extracts were dried over anhydrous magnesium sulfate, filtered, and concentrated in vacuo. The residue was purified by silica gel column chromatography using a gradient mixture of hexane–ethyl acetate (30%–80%), and the product was obtained as white solid (29 mg, 0.08 mmol, 29%). ^{1}H NMR (300 MHz, $CDCl_3$) δ 8.23 (s, 2H), 8.08 (s, 1H), 7.98 (d, J = 2.5 Hz, 1H), 7.66 (d, J = 4.8 Hz, 1H), 7.30 – 7.27 (m, 1H), 5.59 (s, 2H), 3.87 (s, 3H). ^{13}C NMR (75 MHz, $CDCl_3$) δ 159.23, 158.95 (d, J = 250.2 Hz), 149.80, 145.46, 145.17, 133.76 (d, J = 3.6 Hz), 125.84, 121.28, 121.07 (d, J = 7.7 Hz), 117.40 (d, J = 24.1 Hz), 110.22 (d, J = 22.8 Hz), 61.07, 56.52. ^{19}F NMR (282 MHz, $CDCl_3$) δ -102.37. HRMS (*m*/*z*): $[M + Na]^+$ calculated for $C_{14}H_{11}BrFN_5O_2Na^+$, 401.9972, found 401.9978.

Compounds **12**–**14** were synthesized by following the same procedure for **11** described above.

*2-((1-(4-Bromo-3-fluorophenyl)-1H-1,2,3-triazol-4-yl)methoxy)-5-methoxypyrimidine (**12**)*. White solid, yield 30%. ^{1}H NMR (300 MHz, d_6-DMSO) δ 8.96 (s, 1H), 8.40 (s, 2H), 8.06 (d, J = 9.7 Hz, 1H), 7.95 (t, J = 7.5 Hz, 1H), 7.79 (d, J = 8.7 Hz, 1H), 5.46 (s, 2H), 3.84 (s, 3H). ^{13}C NMR (75 MHz, d_6-DMSO) δ 159.15, 159.00 (d, J = 245.4 Hz), 150.02, 146.14, 144.54, 137.46 (d, J = 10.0 Hz), 135.14, 123.50, 117.86 (d, J = 3.5 Hz), 109.37 (d, J = 27.5 Hz), 108.25 (d, J = 20.7 Hz), 60.48, 56.97. ^{19}F NMR (282 MHz, d_6-DMSO) δ -100.92 – -101.00 (m). HRMS (*m*/*z*): $[M + Na]^+$ calculated for $C_{14}H_{11}BrFN_5O_2Na^+$, 401.9972, found 401.9975.

*2-((1-(4-Fluoro-3-methylphenyl)-1H-1,2,3-triazol-4-yl)methoxy)-5-methoxypyrimidine (**13**)*. White solid, yield 30%. ^{1}H NMR (300 MHz, $CDCl_3$) δ 8.23 (s, 2H), 8.05 (s, 1H), 7.58 (s, 1H), 7.46 (s, 1H), 7.13 (t, J = 8.3 Hz, 1H), 5.59 (s, 2H), 3.87 (s, 3H), 2.35 (s, 3H). ^{13}C NMR (75 MHz, $CDCl_3$) δ 160.98 (d, J = 249.8 Hz), 159.32, 149.77, 145.45, 144.74, 132.93, 126.78 (d, J = 19.0 Hz), 123.89 (d, J = 5.5 Hz), 121.42, 119.64 (d, J = 8.6 Hz), 116.10 (d, J = 24.3 Hz), 61.22, 56.53, 14.66 (d, J = 3.3 Hz). ^{19}F NMR (282 MHz, $CDCl_3$) δ -112.34. HRMS (*m*/*z*): $[M + Na]^+$ calculated for

$C_{15}H_{14}FN_5O_2Na^+$, 338.1024, found 338.1029.

2-((1-(3-Fluoro-4-methylphenyl)-1H-1,2,3-triazol-4-yl)methoxy)-5-methoxypyrimidine ***(14)***. White solid, yield 24%. ^{1}H NMR (300 MHz, d_6-DMSO) δ 8.89 (s, 1H), 8.39 (s, 2H), 7.73 (dd, J = 26.9, 9.4 Hz, 2H), 7.49 (t, J = 8.2 Hz, 1H), 5.44 (s, 2H), 3.84 (s, 3H), 2.28 (s, 3H). ^{13}C NMR (75 MHz, d_6-DMSO) δ 161.04 (d, J = 244.4 Hz), 159.18, 150.00, 146.13, 144.23, 136.00 (d, J = 10.3 Hz), 133.13 (d, J = 6.0 Hz), 125.29 (d, J = 17.2 Hz), 123.33, 116.14 (d, J = 3.3 Hz), 107.74 (d, J = 27.5 Hz), 60.53, 56.95, 14.29. ^{19}F NMR (282 MHz, d_6-DMSO) δ -110.48 – -110.55 (m). HRMS (m/z): $[M + Na]^+$ calculated for $C_{15}H_{14}FN_5O_2Na^+$, 338.1024, found 338.1025.

Pharmacology study. Recombinant receptors were expressed from cDNAs encoding human NMDA receptor subunits GluN1-1a (hereafter GluN1; GenBank NP_015566), GluN2A (GenBank NP_000824), GluN2B (GenBank NP_000825), and GluN2D (GenBankNP_000827.1)[65] Rat GluN1-1a (U11418, U08261) and GluN2C (M91563), GluA1-flip (P19490), and GluK2(Q) (P42260) were used for the study of subunit selectivity. cRNA was transcribed in vitro from plasmids containing NMDAR cDNAs.[66] *Xenopus laevis* stage VI oocytes were prepared from commercially available ovaries (Xenopus one Inc, Dexter, MI, USA). The ovary was placed in a petri plate at room temperature, gently pulled apart with two fine forceps and transferred into Collagenase Type 4 (Worthington-Biochem, Lakewood, NJ, USA) solution (850 μg/ml, 15 ml for a half ovary) in Ca^{2+}-free Barth's solution (see below). The ovary was digested on a mixer at room temperature (23 °C) for 2 h. If the oocytes were under digested, they were kept on a mixer for an additional 15 min. The oocytes were then rinsed 5 times with Ca^{2+}-free Barth's on a mixer for 10 min (with 35–40 mL of fresh solution each time), and further rinsed for 4 times with normal Barth's on the mixer for 10 min (35–40 mL of fresh solution each time). The oocytes were placed in petri plates for sorting and kept in a 16°C incubator afterward. The oocytes were injected with 5–10 ng cRNA and stored at 15 °C in media containing (Barth's, in mM) 88 NaCl, 2.4 $NaHCO_3$, 1 KCl, 0.33 $Ca(NO_3)_2$, 0.41 $CaCl_2$, 0.82 $MgSO_4$, 5 HEPES, 1 U/mL penicillin, 0.1 mg/mL gentamicin sulfate, and 1 μg/mL streptomycin (pH 7.4, adjusted with NaOH). Two to seven days after injection, two-electrode voltage-clamp recordings[66] were performed at room temperature in an extracellular

solution containing (in mM) 90 NaCl, 1 KCl, 10 HEPES, 0.5 $BaCl_2$, and 0.01 EDTA (pH 7.4, adjusted with NaOH). NMDAR current responses from oocytes were recorded at a holding potential of -40 mV. Concentration–response curves for GluN2B antagonists were generated by co-applying 100 μM glutamate and 100 μM glycine with variable concentrations of test compounds up to 1 μM. Test compounds were prepared as 20 mM stock solutions in DMSO and diluted to the final concentration in recording solution. DMSO content was 0.05–0.5% (v/v). The response to test compounds was given as a percentage of the initial response to glutamate and glycine alone. Data for individual cells were fitted in OriginPro (v 9.0) with the Hill equation:

$$Response\ (\%) = (100 - minimum)/(1 + ([concentration]/IC_{50})^{N}) + minimum$$

where the *minimum* is the residual response in saturating inhibitor, IC_{50} is the concentration that reduces the response by half, and *N* is the Hill slope. Mean fitted IC_{50} values from individual cells are given with the 95% confidence interval (CI) determined from the $\log(IC_{50})$ was used to determine the CI, which were then transformed back to concentration. For the graphical representation, the data were normalized to the current response to agonist alone, averaged across all cells, and fitted to the Hill equation.

The triheteromeric receptors (2A/2B) and diheterometric receptors (2A/2A and 2B/2B) used here were developed by the method previously reported,[45] and their current amplitude evoked by agonists glutamate/glycine (100 μM/100 μM) was showed in Figure S2 in SI.

Molecular Docking Studies. Candidate compounds **11** and **13** were docked onto the selected protein structure (PDB ID: 3QEL) using the AutoDock Vina module in the UCSF Chimera software. Briefly, the mol2 file of protein was prepared by deleting the solvent, adding hydrogen atoms and charges using the default settings. Standard residues were determined according to the AMBER 14 force field, while non-standard residues were ignored. The predicted free energy of binding was calculated in AutoDock Vina using a hybrid scoring function (combined knowledge-based and empirical approaches).[67]

Radiochemistry. *One-step radiolabeling of [^{18}F]**11***: [^{18}F]F^- on the QMA cartridge was eluted into a 5 mL reaction vial with 1 mL of Kryptofix$_{222}$/K_2CO_3 solution (7.5 mg of Kryptofix$_{222}$ and 1.5 mg

of K_2CO_3 in CH_3CN/H_2O, 4/1, v/v). The solvent was removed, and then the residue was dried azeotropically with anhydrous acetonitrile (1 mL × 3) under a stream of nitrogen at 120 ºC. The vessel was cooled to room temperature, and a solution of nitro precursor **17** (2.5 – 3.5 mg) in anhydrous DMF (1 mL) was added. The reaction mixture was heated to 140 ºC and kept for 10 min. After that, the reaction mixture was purified with HPLC (Waters) using a YMC C18 reverse phase column (5 μm, 10 × 250 mm, elution: CH_3CN/H_2O = 45%/55%, 4 mL/min). To the separated solution of [^{18}F]**11**, 20 mL of water was added, and then passed through a preconditioned Sep-Pak Plus-C18 cartridge (Waters). The cartridge was washed with 10 mL of water, and the labeled compound [^{18}F]**11** was eluted to a glass vial with 1 mL of ethanol. The ethanol eluent was concentrated under nitrogen flow at 60 ºC and then formulated with saline (containing 5%–8% ethanol) for further studies. The radiochemical yield is ~3% (decay corrected), and the radiochemical purity is > 99%.

*Two-step radiolabeling of [^{18}F]**11** and [^{18}F]**13***: [^{18}F]F^- on the QMA cartridge was eluted into a 5 mL reaction vial with 1 mL of TEAB solution (3.5 mg, CH_3CN/H_2O, 7/3, v/v). After [^{18}F]F^- was dried under a nitrogen stream and cooled to room temperature (same procedure as above), a solution of SCIDY precursor **20** or **21** (~5 mg) in anhydrous DMF (400 μL) was added. After the reaction at 120 ºC for 10 min, **16** (2–3 mg), CuI (2–3 mg), and DIPEA (5 μL) were added and the reaction mixture was kept at 100 ºC for another 10 min. Then the reaction mixture was quenched with 10 mL water, passed through a preconditioned Sep-Pak Plus-C18 cartridge (Waters), washed with 10 mL water and eluted with 1–1.5 mL acetonitrile. The eluent was purified with HPLC (Waters) using a YMC C18 reverse phase column (5 μm, 10 × 250 mm, 5 mL/min, elution: CH_3CN/H_2O = 45%/55% and 40%/60% for [^{18}F]**11** and [^{18}F]**13**, respectively). The fraction containing [^{18}F]**11** (or [^{18}F]**13**) was mixed with 20 mL of water and then passed through a preconditioned Sep-Pak Plus-C18 cartridge (Waters). The cartridge was washed with 10 mL of water, and the labeled compound [^{18}F]**11** (or [^{18}F]**13**) was eluted to a reaction vial with 1 mL of ethanol. The ethanol eluent was concentrated under nitrogen flow at 60 ºC and then formulated with saline (containing 5%–8% ethanol) for further studies. The identities of [^{18}F]**11** and [^{18}F]**13** were confirmed with HPLC by the

co-injection with corresponding cold compounds of **11** or **13**, respectively (Figure S1 in Supporting Information).

In Vitro Autoradiography of [^{18}F]13 in Brain Sections of Rat and NHP. Rat brain cryosections (20 μm) were preincubated for 20 min in 50 mM Tris-HCl buffer (pH 7.4) at room temperature. These sections were incubated for 60 min at room temperature with Tris-HCl buffer containing [^{18}F]**13** (37 kBq/mL, 1.58 nM). After incubation, the brain sections were washed with cold buffer (0.5 mL) and dried with cold air. Then the sections were opposed to imaging plates (GE) overnight and autoradiograms were obtained using an Amersham Typhoon 5 (GE) analyzer system with the resolution of 10 μm and sensitivity of 4000. Self-blocking experiment with cold compound of **13** (10 μM, 0.1% DMSO, 1% ethanol in Tris-HCl buffer) was used to determine the nonspecific binding of [^{18}F]**13**: before incubation with [^{18}F]**13**, the sections were incubated with the solution of **13** for 30 min and then washed with cold Tris-HCl buffer (1 mL). In blocking experiments with BMT-108908 (10 μM, 0.1% DMSO, 1% ethanol in Tris-HCl buffer), the same procedure as self-blocking was used. The in vitro ARG in NHP brain sections including baseline, self-blocking, and BMT-108908 blocking experiments were carried out by following the same procedure as described above.

Distribution of radioactivity on the plates was analyzed by ImageJ, in which the regions of interest (ROIs) were placed on the hippocampus, frontal cortex, striatum, thalamus, and cerebellum in rat brain sections, and hippocampus, entorhinal cortex, insular cortex, caudate nucleus, putamen, thalamus and white matter of forebrain in NHP brain sections. The radioactivity in these regions was expressed as gray value/unit area, which is in linear with the radioactivity. The relative radioactivity was represented as the ratio of gray value/unit area (radioactivity) of different brain regions to that of the cerebellum (for rat) or white matter of forebrain (for NHP), where only slight radioactivity was observed.

Whole Body Biodistribution Study and Radiometabolite Analysis in Mice. The CD1 (ICR) mice (female, 8 weeks, 23–27 g) were intravenously injected with [^{18}F]**13** (740 kBq/100 μL in saline containing 5% ethanol) through the tail vein. The mice were sacrificed at various time points

of 2, 10, 30, and 60 min post-injection. The organs of interest were removed and weighed, and the radioactivity was measured with an automatic γ-counter (WALLAC/Wizard 1470, USA). The percent dose per gram (% ID/g) or percent dose per organ (% ID/organ) of wet tissue values were calculated by relating the tissue radioactivity counts to that of suitably diluted aliquots of the injected dose. All radioactivity measurements were decay-corrected.

After intravenous injection of [^{18}F]**13** through tail vein, the mice (n = 2) were sacrificed at 15 min. Blood sample was collected and centrifuged at 14000 rpm for 3 min at 4 °C to separate the plasma. The supernatant was collected and added to an ice-cooled test tube containing 100 μL of CH_3CN. After vortex for 10 s, the mixture was centrifuged at 14000 rpm for 3 min at 4 °C for deproteinization. The supernatant was collected, and the process was repeated until no precipitations were observed when CH_3CN was added. The mice brain was immediately dissected, homogenized with 400 μL of ice-cooled CH_3CN, and then centrifuged at 14000 rpm for 5 min at 4 °C. The supernatant was collected into a test tube containing 100 μL of ice-cooled CH_3CN, and the process (vortex and centrifuge) was repeated until no precipitations were observed when CH_3CN was added. The resulting supernatants of plasma and brain were mixed with 50 μL of a solution of cold compound [^{18}F]**13** and then analyzed on a radioHPLC system using a Phenomenex C18 column (5 μm, 10 × 250 mm, 5 mL/min, elution: CH_3CN/H_2O = 55%/45%). The radioactivity was collected and counted using 1480 Wizard gamma counter (PerkinElmer, USA). The radioactivity overlapped with [^{18}F]**13** in the UV signal corresponded to that of [^{18}F]**13** (t_R = 6.90 min). The percentage of [^{18}F]**13** to total radioactivity was calculated as (counts for [^{18}F]**13**/total counts) × 100. The whole body biodistribution study and radiometabolite analysis in mice of [^{18}F]**11** were conducted by following the same procedures for [^{18}F]**13**.

ASSOCIATED CONTENT

Characterization of all new compounds and NMR spectra; ex vivo biodistribution data. This material is available free of charge via the Internet at http://pubs.acs.org.

AUTHOR INFORMATION

Corresponding Author

*S.H.L.: tel: +1 617 726 6107; fax, +1 617 726 6165; e-mail, liang.steven@mgh.harvard.edu.

*S.F.T.: tel, +1 404-727-1375; fax, +1 404-727-0365; e-mail, strayne@emory.edu.

*Z.L.: tel, +86 592 2880645; fax, +86 592 2880645; e-mail, zijing.li@xmu.edu.cn.

Author Contributions

The manuscript was written through contributions of all authors. All authors have read and approved the final version.

Notes

S.F.T. is a consultant for Janssen Pharmaceuticals Inc., is PI on a research grant from Janssen to Emory University School of Medicine, is a member of the SAB for Sage Therapeutics, is co-founder of NeurOp Inc, and receives royalties for software. S.F.T. is co-inventor on Emory-owned Intellectual Property that includes allosteric modulators of NMDA receptor function. H.Y. is PI on a research grant from Sage Therapeutics to Emory University School of Medicine. The other authors declare no competing financial interest.

ACKNOWLEDGMENT

We thank Dr. Lei Zhang (Medicine Design, Pfizer, Inc) and Professor Thomas J. Brady (Nuclear Medicine and Molecular Imaging, Radiology, MGH and Harvard Medical School) for helpful discussion. Z.L. acknowledges financial supports from the National Natural Science Foundation of China (81501534), Fourth Round Fujian Health Education Joint Research Projects (WKJ2016-2-08), Fundamental Research Funds for the Central Universities (20720180050), Fujian Province Young Teacher Research Program (JA15010) and Scientific Research Foundation of State Key Laboratory of Molecular Vaccinology and Molecular Diagnostics (2016ZY002). Financial support from the NIH grants (NINDS NS065371 to S.F.T.; NICHD HD082373 to H.Y.; NIAAA AA019431

to J.B.D. and NIAAA AA014106 to David P. Friedman) is gratefully acknowledged.

ABBREVIATIONS

AD, Alzheimer's disease; ARG, autoradiography; BBB, blood-brain barrier; CI, confidence interval; CNS, central nervous system; HPLC, high-performance liquid chromatography; iGluRs, ionotropic glutamate receptors; MPO, multiparameter optimization; NAM, negative allosteric modulators; NMDAR, *N*-methyl-D-aspartate receptors; NHP, non-human primates; PAINS, Pan Assay Interference Compounds Assay; PAM, positive allosteric modulators; PCP, phencyclidine; PET, positron emission tomography; RCY, radiochemistry yield; ROI, region of interest; SCIDY, spirocyclic iodonium ylide; S_NAr, nucleophilic aromatic substitution; TLC, thin-layer chromatography; tPSA, topological polar surface area.

REFERENCES

1. Paoletti, P., Bellone, C., and Zhou, Q. (2013) NMDA receptor subunit diversity: impact on receptor properties, synaptic plasticity and disease, *Nat. Rev. Neurosci. 14*, 383-400.
2. Traynelis, S. F., Wollmuth, L. P., McBain, C. J., Menniti, F. S., Vance, K. M., Ogden, K. K., Hansen, K. B., Yuan, H., Myers, S. J., and Dingledine, R. (2010) Glutamate receptor ion channels: structure, regulation, and function, *Pharmacol. Rev. 62*, 405-496.
3. Parsons, M. P., and Raymond, L. A. (2014) Extrasynaptic NMDA receptor involvement in central nervous system disorders, *Neuron 82*, 279-293.
4. Gonzalez, J., Jurado-Coronel, J. C., Avila, M. F., Sabogal, A., Capani, F., and Barreto, G. E. (2015) NMDARs in neurological diseases: a potential therapeutic target, *Int. J. Neurosci. 125*, 315-327.
5. Chazot, P. L. (2004) The NMDA receptor NR2B subunit: a valid therapeutic target for multiple CNS pathologies, *Curr. Med. Chem. 11*, 389-396.
6. Ogden, K. K., and Traynelis, S. F. (2011) New advances in NMDA receptor pharmacology, *Trends Pharmacol. Sci. 32*, 726-733.
7. Kemp, J. A., and McKernan, R. M. (2002) NMDA receptor pathways as drug targets, *Nat. Neurosci. 5*, 1039-1042.
8. Mony, L., Kew, J. N., Gunthorpe, M. J., and Paoletti, P. (2009) Allosteric modulators of NR2B-containing NMDA receptors: molecular mechanisms and therapeutic potential, *Br. J. Pharmacol. 157*, 1301-1317.
9. Kemp, J.A., Kew, J.N.C., Gill, R. (1999) NMDA Receptor Antagonists and Their Potential as

Neuroprotective Agents. In *Ionotropic Glutamate Receptors in the CNS. Handbook of Experimental Pharmacology* (Jonas, P., and Monyer, H., Ed.), pp 495–527, Springer, Berlin.

10. Madden, D. R. (2002) The structure and function of glutamate receptor ion channels, *Nat. Rev. Neurosci. 3*, 91-101.

11. Monyer, H., Burnashev, N., Laurie, D. J., Sakmann, B., and Seeburg, P. H. (1994) Developmental and regional expression in the rat brain and functional properties of four NMDA receptors, *Neuron 12*, 529-540.

12. Sheng, M., Cummings, J., Roldan, L. A., Jan, Y. N., and Jan, L. Y. (1994) Changing subunit composition of heteromeric NMDA receptors during development of rat cortex, *Nature 368*, 144-147.

13. Paoletti, P. (2011) Molecular basis of NMDA receptor functional diversity, *Eur. J. Neurosci. 33*, 1351-1365.

14. Watanabe, M., Inoue, Y., Sakimura, K., and Mishina, M. (1992) Developmental changes in distribution of NMDA receptor channel subunit mRNAs, *Neuroreport 3*, 1138-1140.

15. Akazawa, C., Shigemoto, R., Bessho, Y., Nakanishi, S., and Mizuno, N. (1994) Differential expression of five *N*-methyl-D-aspartate receptor subunit mRNAs in the cerebellum of developing and adult rats, *J. Comp. Neurol. 347*, 150-160.

16. Zhu, S., and Paoletti, P. (2015) Allosteric modulators of NMDA receptors: multiple sites and mechanisms, *Curr. Opin. Pharmacol. 20*, 14-23.

17. Karakas, E., Simorowski, N., and Furukawa, H. (2009) Structure of the zinc-bound amino-terminal domain of the NMDA receptor NR2B subunit, *EMBO J. 28*, 3910-3920.

18. Karakas, E., Simorowski, N., and Furukawa, H. (2011) Subunit arrangement and phenylethanolamine binding in GluN1/GluN2B NMDA receptors, *Nature 475*, 249-253.

19. Mony, L., Zhu, S., Carvalho, S., and Paoletti, P. (2011) Molecular basis of positive allosteric modulation of GluN2B NMDA receptors by polyamines, *EMBO J. 30*, 3134-3146.

20. Loftis, J. M., and Janowsky, A. (2003) The *N*-methyl-D-aspartate receptor subunit NR2B: localization, functional properties, regulation, and clinical implications, *Pharmacol. Ther. 97*, 55-85.

21. Hu, C., Chen, W., Myers, S. J., Yuan, H., and Traynelis, S. F. (2016) Human GRIN2B variants in neurodevelopmental disorders, *J. Pharmacol. Sci. 132*, 115-121.

22. Chenard, B. L., and Menniti, F. S. (1999) Antagonists selective for NMDA receptors containing the NR2B subunit, *Curr. Pharm. Des. 5*, 381-404.

23. Kew, J. N., Trube, G., and Kemp, J. A. (1996) A novel mechanism of activity-dependent NMDA receptor antagonism describes the effect of ifenprodil in rat cultured cortical neurones, *J. Physiol. 497 (Pt 3)*, 761-772.

24. Stroebel, D., Buhl, D. L., Knafels, J. D., Chanda, P. K., Green, M., Sciabola, S., Mony, L., Paoletti, P., and Pandit, J. (2016) A Novel Binding Mode Reveals Two Distinct Classes of NMDA Receptor GluN2B-selective Antagonists, *Mol. Pharmacol. 89*, 541-551.

25. Burger, P. B., Yuan, H., Karakas, E., Geballe, M., Furukawa, H., Liotta, D. C., Snyder, J. P., and Traynelis, S. F. (2012) Mapping the binding of GluN2B-selective *N*-methyl-D-aspartate receptor negative allosteric modulators, *Mol. Pharmacol. 82*, 344-359.

26. Chazot, P. L. (2000) CP-101606 Pfizer Inc, *Curr. Opin. Investig. Drugs 1*, 370-374.
27. Yurkewicz, L., Weaver, J., Bullock, M. R., and Marshall, L. F. (2005) The effect of the selective NMDA receptor antagonist traxoprodil in the treatment of traumatic brain injury, *J. Neurotrauma 22*, 1428-1443.
28. Ibrahim, L., Diaz Granados, N., Jolkovsky, L., Brutsche, N., Luckenbaugh, D. A., Herring, W. J., Potter, W. Z., and Zarate, C. A., Jr. (2012) A Randomized, placebo-controlled, crossover pilot trial of the oral selective NR2B antagonist MK-0657 in patients with treatment-resistant major depressive disorder, *J. Clin. Psychopharmacol. 32*, 551-557.
29. Garner, R., Gopalakrishnan, S., McCauley, J. A., Bednar, R. A., Gaul, S. L., Mosser, S. D., Kiss, L., Lynch, J. J., Patel, S., Fandozzi, C., Lagrutta, A., Briscoe, R., Liverton, N. J., Paterson, B. M., Vornov, J. J., and Mazhari, R. (2015) Preclinical pharmacology and pharmacokinetics of CERC-301, a GluN2B-selective *N*-methyl-D-aspartate receptor antagonist, *Pharmacol. Res. Perspect. 3*, e00198.
30. Santangelo, R. M., Acker, T. M., Zimmerman, S. S., Katzman, B. M., Strong, K. L., Traynelis, S. F., and Liotta, D. C. (2012) Novel NMDA receptor modulators: an update, *Expert Opin. Ther. Pat. 22*, 1337-1352.
31. Sobrio, F., Gilbert, G., Perrio, C., Barre, L., and Debruyne, D. (2010) PET and SPECT imaging of the NMDA receptor system: an overview of radiotracer development, *Mini. Rev. Med. Chem. 10*, 870-886.
32. Majo, V. J., Prabhakaran, J., Mann, J. J., and Kumar, J. S. (2013) PET and SPECT tracers for glutamate receptors, *Drug Discov. Today 18*, 173-184.
33. Fu, H., Chen, Z., Josephson, L., Li, Z., and Liang, S. H. (2018) Positron Emission Tomography (PET) Ligand Development for Ionotropic Glutamate Receptors: Challenges and Opportunities for Radiotracer Targeting *N*-Methyl-D-aspartate (NMDA), alpha-Amino-3-hydroxy-5-methyl-4-isoxazolepropionic Acid (AMPA), and Kainate Receptors, *J. Med. Chem.*, DOI: 10.1021/acs.jmedchem.1028b00714.
34. Haradahira, T., Maeda, J., Okauchi, T., Zhang, M. R., Hojo, J., Kida, T., Arai, T., Yamamoto, F., Sasaki, S., Maeda, M., Suzuki, K., and Suhara, T. (2002) Synthesis, in vitro and in vivo pharmacology of a C-11 labeled analog of CP-101,606, (+/-)threo-1-(4-hydroxyphenyl)-2-[4-hydroxy-4-(p-[^{11}C]methoxyphenyl)piperidino]-1 -propanol, as a PET tracer for NR2B subunit-containing NMDA receptors, *Nucl. Med. Biol. 29*, 517-525.
35. Roger, G., Dolle, F., De Bruin, B., Liu, X., Besret, L., Bramoulle, Y., Coulon, C., Ottaviani, M., Bottlaender, M., Valette, H., and Kassiou, M. (2004) Radiosynthesis and pharmacological evaluation of [^{11}C]EMD-95885: a high affinity ligand for NR2B-containing NMDA receptors, *Bioorg. Med. Chem. Lett. 12*, 3229-3237.
36. Dollé, F., Valette, H., Demphel, S., Coulon, C., Ottaviani, M., Bottlaender, M., and Kassiou, M. (2004) Radiosynthesis and in vivo evaluation of [^{11}C]Ro-647312: a novel NR1/2B subtype selective NMDA receptor radioligand, *J. Labelled Compd. Radiopharm. 47*, 911-920.
37. Arstad, E., Platzer, S., Berthele, A., Pilowsky, L. S., Luthra, S. K., Wester, H. J., and Henriksen, G. (2006) Towards NR2B receptor selective imaging agents for PET-synthesis and evaluation of *N*-[^{11}C]-(2-methoxy)benzyl (*E*)-styrene-, 2-naphthyl- and 4-trifluoromethoxyphenylamidine,

Bioorg. Med. Chem. Lett. 14, 6307-6313.
38. Koudih, R., Gilbert, G., Dhilly, M., Abbas, A., Barre, L., Debruyne, D., and Sobrio, F. (2012) Synthesis and in vitro characterization of trans- and cis-[^{18}F]-4-methylbenzyl 4-[(pyrimidin-2-ylamino)methyl]-3-fluoropiperidine-1-carboxylates as new potential PET radiotracer candidates for the NR2B subtype *N*-methyl-D-aspartate receptor, *Eur. J. Med. Chem. 53*, 408-415.
39. Koudih, R., Gilbert, G., Dhilly, M., Abbas, A., Barre, L., Debruyne, D., and Sobrio, F. (2012) Radiolabelling of 1,4-disubstituted 3-[^{18}F]fluoropiperidines and its application to new radiotracers for NR2B NMDA receptor visualization, *Org. Biomol. Chem. 10*, 8493-8500.
40. Krämer, S. D., Betzel, T., Mu, L., Haider, A., Herde, A. M., Boninsegni, A. K., Keller, C., Szermerski, M., Schibli, R., Wünsch, B., and Ametamey, S. M. (2018) Evaluation of ^{11}C-Me-NB1 as a potential PET radioligand for measuring GluN2B-containing NMDA receptors, drug occupancy, and receptor cross talk, *J. Nucl. Med. 59*, 698-703.
41. Cai, L., Liow, J.-S., Morse, C., Davies, R., Frankland, M., Zoghbi, S., Innis, R., and Pike, V. (2018) Synthesis of [^{11}C]NR2B-SMe for evaluation as a PET radioligand for NR2B subunits in NMDA receptors, *J. Nucl. Med. 59*, 543.
42. Chen, G., Chrovian, C. C., Coate, H. R., Dvorak, C. A., Gelin, C. F., Hiscox, A., Letavic, M. A., Rech, J. C., Soyode-Johnson, A., and Stenne, B. (2017) Substituted 1,2,3-triazoles as NR2B-selective NMDA modulators, Internatinal Patent Application, WO 2017/139428 A139421.
43. Rotstein, B. H., Stephenson, N. A., Vasdev, N., and Liang, S. H. (2014) Spirocyclic hypervalent iodine(III)-mediated radiofluorination of non-activated and hindered aromatics, *Nat. Commun. 5*, 4365.
44. Rotstein, B. H., Wang, L., Liu, R. Y., Patteson, J., Kwan, E. E., Vasdev, N., and Liang, S. H. (2016) Mechanistic Studies and Radiofluorination of Structurally Diverse Pharmaceuticals with Spirocyclic Iodonium(III) Ylides, *Chem. Sci. 7*, 4407-4417.
45. Hansen, K. B., Ogden, K. K., Yuan, H., and Traynelis, S. F. (2014) Distinct functional and pharmacological properties of Triheteromeric GluN1/GluN2A/GluN2B NMDA receptors, *Neuron 81*, 1084-1096.
46. Waterhouse, R. N. (2003) Determination of lipophilicity and its use as a predictor of blood–brain barrier penetration of molecular imaging agents, *Mol. Imaging Biol. 5*, 376-389.
47. Pike, V. W. (2016) Considerations in the Development of Reversibly Binding PET Radioligands for Brain Imaging, *Curr. Med. Chem. 23*, 1818-1869.
48. Pike, V. W. (2009) PET radiotracers: crossing the blood-brain barrier and surviving metabolism, *Trends Pharmacol. Sci. 30*, 431-440.
49. Test No. 107: Partition Coefficient (n-Octanol/Water): Shake Flask Method. *Guidelines for the Testing of Chemicals, Section 1*; Organisation for Economic Cooperation and Development (OECD): Paris, 1995; DOI: 10.1787/9789264069626-en.
50. Hitchcock, S. A., and Pennington, L. D. (2006) Structure-brain exposure relationships, *J. Med. Chem. 49*, 7559-7583.
51. Wager, T. T., Hou, X., Verhoest, P. R., and Villalobos, A. (2010) Moving beyond rules: the development of a central nervous system multiparameter optimization (CNS MPO) approach to enable alignment of druglike properties, *ACS Chem. Neurosci. 1*, 435-449.

52. Wager, T. T., Hou, X., Verhoest, P. R., and Villalobos, A. (2016) Central Nervous System Multiparameter Optimization Desirability: Application in Drug Discovery, *ACS Chem. Neurosci. 7*, 767-775.

53. Zhang, L., Villalobos, A., Beck, E. M., Bocan, T., Chappie, T. A., Chen, L., Grimwood, S., Heck, S. D., Helal, C. J., Hou, X., Humphrey, J. M., Lu, J., Skaddan, M. B., McCarthy, T. J., Verhoest, P. R., Wager, T. T., and Zasadny, K. (2013) Design and selection parameters to accelerate the discovery of novel central nervous system positron emission tomography (PET) ligands and their application in the development of a novel phosphodiesterase 2A PET ligand, *J. Med. Chem. 56*, 4568-4579.

54. Deng, X., Rong, J., Wang, L., Vasdev, N., Zhang, L., Josephson, L., and Liang, S. (2018) Chemistry for Positron Emission Tomography: Recent Advances in ^{11}C-, ^{18}F-, ^{13}N- and ^{15}O-labeling Reactions, *Angew. Chem. Int. Ed. Engl.*, DOI: 10.1002/anie.201805501.

55. Shen, B., Löffler, D., Reischl, G., Machulla, H.-J., and Zeller, K.-P. (2010) Nucleophilic [^{18}F]Fluorination and subsequent decarbonylation of methoxy-substituted nitro- and halogen-benzenes activated by one or two formyl groups, *J. Labelled Compd. Radiopharm. 53*, 113-119.

56. Cai, L., Lu, S., and Pike, V. W. (2008) Chemistry with [^{18}F]Fluoride Ion, *Eur. J. Org. Chem. 2008*, 2853-2873.

57. Agalave, S. G., Maujan, S. R., and Pore, V. S. (2011) Click Chemistry: 1,2,3-Triazoles as Pharmacophores, *Chem. - Asian J. 6*, 2696-2718.

58. Menniti, F., Chenard, B., Collins, M., Ducat, M., Shalaby, I., and White, F. (1997) CP-101,606, a potent neuroprotectant selective for forebrain neurons, *Eur. J. Pharmacol. 331*, 117-126.

59. Mori, H., and Mishina, M. (1995) Structure and function of the NMDA receptor channel, *Neuropharmacology 34*, 1219-1237.

60. Marcin, L. R., Warrier, J., Thangathirupathy, S., Shi, J., Karageorge, G. N., Pearce, B. C., Ng, A., Park, H., Kempson, J., Li, J., Zhang, H., Mathur, A., Reddy, A. B., Nagaraju, G., Tonukunuru, G., Gupta, G., Kamble, M., Mannoori, R., Cheruku, S., Jogi, S., Gulia, J., Bastia, T., Sanmathi, C., Aher, J., Kallem, R., Srikumar, B. N., Vijaya, K. K., Naidu, P. S., Paschapur, M., Kalidindi, N., Vikramadithyan, R., Ramarao, M., Denton, R., Molski, T., Shields, E., Subramanian, M., Zhuo, X., Nophsker, M., Simmermacher, J., Sinz, M., Albright, C., Bristow, L. J., Islam, I., Bronson, J. J., Olson, R. E., King, D., Thompson, L. A., and Macor, J. E. (2018) BMS-986163, a Negative Allosteric Modulator of GluN2B with Potential Utility in Major Depressive Disorder, *ACS Med. Chem. Lett. 9*, 472-477.

61. Weed, M. R., Bookbinder, M., Polino, J., Keavy, D., Cardinal, R. N., Simmermacher-Mayer, J., Cometa, F.-n. L., King, D., Thangathirupathy, S., Macor, J. E., and Bristow, L. J. (2015) Negative Allosteric Modulators Selective for The NR2B Subtype of The NMDA Receptor Impair Cognition in Multiple Domains, *Neuropsychopharmacology 41*, 568-577.

62. Baell, J. B., and Holloway, G. A. (2010) New substructure filters for removal of pan assay interference compounds (PAINS) from screening libraries and for their exclusion in bioassays, *J. Med. Chem. 53*, 2719-2740.

63. Daina, A., Michielin, O., and Zoete, V. (2017) SwissADME: a free web tool to evaluate pharmacokinetics, drug-likeness and medicinal chemistry friendliness of small molecules, *Sci. Rep.*

7, 42717.
64. Boechat, N., Ferreira, V. F., Ferreira, S. B., de Lourdes, G. F. M., de, C. d. S. F., Bastos, M. M., Dos, S. C. M., Lourenco, M. C., Pinto, A. C., Krettli, A. U., Aguiar, A. C., Teixeira, B. M., da Silva, N. V., Martins, P. R., Bezerra, F. A., Camilo, A. L., da Silva, G. P., and Costa, C. C. (2011) Novel 1,2,3-triazole derivatives for use against Mycobacterium tuberculosis H37Rv (ATCC 27294) strain, *J. Med. Chem. 54*, 5988-5999.
65. Hedegaard, M., Hansen, K. B., Andersen, K. T., Brauner-Osborne, H., and Traynelis, S. F. (2012) Molecular pharmacology of human NMDA receptors, *Neurochem. Int. 61*, 601-609.
66. Chen, W., Tankovic, A., Burger, P. B., Kusumoto, H., Traynelis, S. F., and Yuan, H. (2017) Functional Evaluation of a De Novo GRIN2A Mutation Identified in a Patient with Profound Global Developmental Delay and Refractory Epilepsy, *Mol. Pharmacol. 91*, 317-330.
67. Trott, O., and Olson, A. J. (2010) AutoDock Vina: improving the speed and accuracy of docking with a new scoring function, efficient optimization, and multithreading, *J. Comput. Chem. 31*, 455-461.

For Table of Contents Use Only

Synthesis and Preliminary Evaluations of a Triazole-cored Antagonist ([^{18}F]N2B-0518) as PET Imaging Probe for GluN2B Subunit in the Brain

Hualong Fu,[†] Weiting Tang,[§,○] Zhen Chen,[†] Vasily V. Belov,[‖] Genwei Zhang,[⊥] Tuo Shao,[†] Xiaofei Zhang,[†] Qingzhen Yu,[†] Jian Rong,[†] Xiaoyun Deng,[†] Wei Han,[§,□] Scott J. Myers,[§] Pilar Giffenig,[‖] Lu Wang,[†,Δ] Lee Josephson,[†] Yihan Shao,[⊥] April T. Davenport,[#] James B. Daunais,[#] Mikhail Papisov,[‖] Hongjie Yuan,[§] Zijing Li,*[,‡] Stephen F. Traynelis,*[,§] and Steven H. Liang*[,†]